Simultaneous Reduction of Co3+ and Mn4+ in P2-Na2/3Co2/3Mn1/3O2 As Evidenced by X-ray Absorption Spectroscopy during Electrochemical Sodium Intercalation

ARTICLE *in* CHEMISTRY OF MATERIALS · JANUARY 2014

Impact Factor: 8.35 · DOI: 10.1021/cm403597h

CHEMISTRY OF MATERIALS

Article

pubs.acs.org/cm

Simultaneous Reduction of Co^{3+} and Mn^{4+} in P2-$Na_{2/3}Co_{2/3}Mn_{1/3}O_2$ As Evidenced by X-ray Absorption Spectroscopy during Electrochemical Sodium Intercalation

Ju-Hsiang Cheng,[†] Chun-Jern Pan,[†] Jyh-Fu Lee,[‡] Jin-Ming Chen,[‡] Marie Guignard,[§] C. Delmas,[§] Dany Carlier,*[,§] and Bing-Joe Hwang*[,†,‡]

[†]Department of Chemical Engineering, National Taiwan University of Science and Technology (NTUST), Taipei 106, Taiwan

[‡]National Synchrotron Radiation Research Center (NSRRC), Hsinchu 30076, Taiwan

[§]CNRS, Université Bordeaux, ICMCB, UPR 9048, F-33600 Pessac, France

Supporting Information

ABSTRACT: Sodium intercalation in P2-$Na_{2/3}Co_{2/3}Mn_{1/3}O_2$ (obtained by a coprecipitation method) was investigated by ex situ and in situ X-ray absorption spectroscopy. The electronic transitions at the O K-edge and the charge compensation mechanism, during the sodium intercalation process, were elucidated by combining Density Function Theory (DFT) calculations and X-ray absorption spectroscopy (XAS) data. The pre-edge of the oxygen K-edge moves to higher energy while the integrated intensity dramatically decreases, indicating that the population of holes in O 2p states is reduced with increasing numbers of sodium ions. From the K-edge and L-edge observations, the oxidation states of pristine Co and Mn were determined to be +III and +IV, respectively. The absorption energy shifts to lower positions during the discharging process for both the Co and the Mn edges, suggesting that the redox pairs, that is, Co^{3+}/Co^{2+} and Mn^{4+}/Mn^{3+}, are both involved in the reaction.

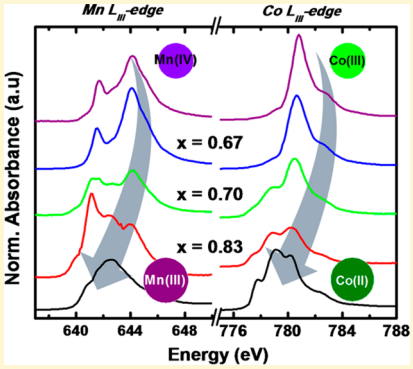

INTRODUCTION

Layered oxides are commonly used as positive electrode materials for both alkaline (nickel hydroxide derivatives) and lithium-ion ($LiCoO_2$ and $LiNiO_2$) secondary batteries. In the case of lithium-ion batteries, the starting material is always in the reduced state as cycling commences with the transition metal ions being initially oxidized during charging before returning to their initial, that is, reduced state, during discharge. The two main parameters that determine a battery's specific energy are directly related to the redox couple involved during charging, and, as several transition metals are involved, the relative oxidation levels of each redox couple are important. The redox potential of a given cation depends both on its intrinsic properties and also on the crystal field imposed by other cations. For example, in the case of the layered $A_x(M,L)O_2$ system, each MO_6 octahedron shares edges with 6 $(M,L)O_6$ octahedra. If there is a significant difference in the ionic radii of the M and L cations, which can increase during charging (noting that the formation of M^{m+} and L^{n+} can promote selective oxidation), unusual electronic configurations may result: for example, in $Li(Ni,Co,Fe)O_2$ systems, partial oxidation of the trivalent iron atom to a Fe^{4+} state has been shown unambiguously by Mössbauer spectroscopy.[1] Similarly, in the case of iron substituted nickel oxyhydroxide used as the positive electrode in alkaline Ni−Cd or Ni−MH batteries, Fe^{4+} ions were also obtained.[2] In the case of the T$^{\#}$2-$Li_{2/3}Co_{2/3}Mn_{1/3}O_2$ phase obtained by ion-exchange from P2-$Na_{2/3}Co_{2/3}Mn_{1/3}O_2$, X-ray absorption near edge spectroscopy (XANES) revealed that the Mn^{4+} and Co^{3+} ions were both reduced during the discharge process.[3] Recently, we have investigated the P2-$Na_{2/3}Mn_{1/3}Co_{2/3}O_2$ phase as a positive electrode in a Na battery. Magnetic susceptibility measurements, electron spin resonance (ESR), and ^{23}Na magic angle spinning nuclear magnetic resonance (MAS NMR) spectroscopy indicated that charge compensation in P2-$Na_{2/3}Co_{2/3}Mn_{1/3}O_2$ is achieved by the stabilization of low-spin Co^{3+} and Mn^{4+} ions,[4] while Na^+ extraction occurs with the oxidation of Co^{3+} to Co^{4+}; however, the nature of the active cation(s) during discharge remains unresolved.

X-ray absorption spectroscopy (XAS) investigations can provide insights into variation of local structures, and oxidation states, during cycling.[5,6] A lot of effort has been directed toward understanding analogous lithiated materials; however, XAS studies on sodium-based battery materials are relatively rare.[7] In this Article, the behavior of P2-$Na_{2/3}Mn_{1/3}Co_{2/3}O_2$ in sodium batteries is examined with a special focus on the XAS characterization of intercalated materials using both ex situ and in situ techniques.

Received: October 30, 2013
Revised: December 12, 2013

   dx.doi.org/10.1021/cm403597h | Chem. Mater. XXXX, XXX, XXX−XXX

EXPERIMENTAL SECTION

$Na_{2/3}Co_{2/3}Mn_{1/3}O_2$ was prepared by a coprecipitation method. In brief, a solution of transition metal nitrates [2/3 of $Co(NO_3)_2{\cdot}6H_2O$ (Fluka) and 1/3 of $Mn(NO_3)_2{\cdot}4H_2O$ (Fluka)] was added progressively to a solution of NaOH (1 M)−NH_4OH (3 M) (with a 5% excess of sodium). Water was then removed by rotary evaporation overnight, and the resulting powder was dried at 110 °C. Heat treatment at 950 °C, for 12 h under O_2, was followed by rapid quenching of the sample in liquid nitrogen.

After complete dissolution of the powder into a hydrochloric acid solution, the material's chemical composition was confirmed, using an ICP-OES spectrometer (Varian 720-ES optical emission spectrometer), as being $Na_{0.68(5)}Co_{0.65(5)}Mn_{0.33(5)}O_2$.

The XRD patterns of the $Na_xCo_{2/3}Mn_{1/3}O_2$ phases were recorded using a Phillips PW1050 powder diffractometer with Cu Kα radiation and a graphite diffracted beam monochromator, from 5° to 120° (2θ) with a 0.02° step (10 s holding time for each step). The unit cell parameters were determined after refining the XRD patterns using the Rietveld method in the Fullprof program.[8]

The electrochemical properties were studied with $Na/NaClO_4$ (1 M) in a propylene carbonate (PC)/$Na_{2/3}Co_{2/3}Mn_{1/3}O_2$ cell. The positive electrode was comprised of a mixture of 84 wt % active material, 11 wt % carbon, and 5 wt % polytetrafluoroethylene (PTFE). The cells were assembled in an argon filled glovebox. The cycling tests were performed starting with charging or discharging in the 1.25−4.0 V vs Na^+/Na potential range with a $C/100$ cycling rate (i.e., 100 h is required to remove one mole of Na^+ ions), this being the same current rate applied for in situ XAS measurements. The samples for soft X-ray absorption were prepared by an ex situ process. The electrodes were charged or discharged to certain voltage and then removed from the batteries and washed using DMC in an argon filled glovebox.

XAS spectra were performed at the National Synchrotron Radiation Research Center (NSRRC), Hsinchu, Taiwan, where the storage ring of the electronic accelerator can supply 1.5 GeV with an operating current of 360 mA. Hard X-ray absorption data for the Co and Mn K-edges were collected at the beamline BL17C. A Si double crystal monochromator was used to perform the energy scan, in which the parallelism was adjusted to eliminate high order harmonics. All of the spectra were recorded using the transmission mode. Ionization chambers were used as detectors to monitor the intensity of the incident and transmitted beams through the specimen, thereby allowing the absorption coefficient to be calculated from the logarithm of the intensity ratio of the incident and transmitted beams. Mn and Co reference foils were positioned in front of the third ionization chamber's window to allow for simultaneous measurement to act as a standard, that is, calibration energy, for each scan. The beam size was limited by the horizontal and vertical slits to an area of 2 × 2 mm^2 during in situ XAS measurements. For the pristine $Na_{2/3}Co_{2/3}Mn_{1/3}O_2$ electrode, the edge jumps for different absorbing species, that is, Co or Mn, were determined from the X-ray absorption near-edge spectroscopy (XANES) spectra.

Standard procedures were followed to analyze the extended X-ray absorption fine structure (EXAFS) data[9] using Athena software:[10] first, the raw absorption spectrum in the pre-edge region was fitted to a straight line and the background above the edge was fitted with a cubic spline. The EXAFS function x was obtained by subtracting the postedge background from the overall absorption and then normalized with respect to the edge jump step. The normalized $\chi(E)$ was transformed from energy space to k space, where k is the photoelectron wave vector. The $\chi(k)$ data could be used to describe the oscillation of the backscattering wave through the local environment. For the $Na_{2/3}Co_{2/3}Mn_{1/3}O_2$ cathode material, k^3-weighted EXAFS spectra [$k^3 \times \chi(k)$] for the selected absorbers, that is, Co and Mn, were calculated to compensate for the damping of EXAFS oscillations in the high-k region. Subsequently, k^3-weighted $x(k)$ data in the k-space ranging from 3.5 to 12.0 $Å^{-1}$ for the Mn K-edge, and 3.5 to 14.0 $Å^{-1}$ for the Co K-edge, were Fourier transformed (FT) to r-space to separate the EXAFS contributions from different coordination shells. A nonlinear least-squares algorithm was applied to the curve fitting of an EXAFS in r space between ∼1.0 and 3.0 Å (depending on the bond to be fitted).

Soft X-ray absorption measurements were made in the X-ray total electron yield mode, for Co and Mn $L_{II,III}$-edges, and in fluorescence mode for the oxygen K-edge using a ultrahigh-vacuum (UHV) chamber with a base pressure of 1 × 10^{-10} Torr. A 6 m high energy spherical grating monochromator (6m-HSGM) was used to perform the energy scan. The depth of the fluorescence mode (giving surface information) and the total electron yield mode (giving information related to the bulk of the particle) are ∼3000 and <50 Å, respectively.[11] However, the 3d transition metals Co and Mn can distort the $L_{II,III}$-edge spectra, due to the self-absorption effect.[12] Therefore, the TEY mode was chosen to measure the Co- and Mn $L_{II,III}$-edges.

First principle calculations were performed using Density Functional Theory with the Vienna ab initio Simulation Package (VASP) code.[13] A plane wave basis set with a cutoff energy of 600 eV was chosen, and PAW potentials were used.[14,15] A supercell was built based on the hexagonal unit cell (P2 stacking) allowing us to perform calculations for the $Na_{2/3}Co_{2/3}Mn_{1/3}O_2$ composition. A $\sqrt{3} \times \sqrt{3}$ in-plane ordering of the Co and Mn ions was employed, and the Na ions were placed in the Na(1) and Na(2) sites in a 1:2 ratio (see Figure S1, Supporting Information). The cell parameters and atomic positions were relaxed using VASP, and reciprocal space sampling was performed with a 6 × 6 × 6 Monkhorst pack k-point grid. All calculations were spin polarized type with ferromagnetic type ordering.

RESULTS AND DISCUSSION

Pure P2-$Na_{2/3}Co_{2/3}Mn_{1/3}O_2$ was prepared and examined by XRD. The pattern shown in Figure S2 (Supporting Information) can be indexed in the hexagonal system using the $P6_3/mmc$ space group. The refined structural parameters are given in Table 1. More details of the XRD refinement used can be found in ref 4.

Table 1. Structural Parameters Obtained from Rietveld Refinement

space group: $P6_3/mmc$, a_{hex} = 2.8286(2) Å, c_{hex} = 11.0398(5) Å					
atom	site	Wyckoff position			occupancy
Na(1)	2b	0	0	1/4	0.26(2)
Na(2)	2d	2/3	1/3	1/4	0.43(2)
Co(1)	2a	0	0	0	0.6667
Mn(1)	2a	0	0	0	0.3333
O(1)	4f	1/3	2/3	0.090(1)	1.0000

Figure 1 shows the electrochemical behavior of P2-$Na_{2/3}Co_{2/3}Mn_{1/3}O_2$, as a positive electrode, in sodium cells with the cycling curve being recorded between 1.25 and 4.0 V, starting with a discharge (not shown) and charge. The charging curve shows a shape identical to that reported in the literature[4,16] with one large and one small potential jump at $x \approx 0.67$ and 0.5. The shape of the charging observed around $x = 1/2$ may be due to the formation of a $Na_{1/2}Co_{2/3}Mn_{1/3}O_2$ phase with Na^+/vacancy ordering. To follow the redox process that is associated with the intercalation of the Na^+ ions in $Na_{2/3}Co_{2/3}Mn_{1/3}O_2$, we studied it using in situ and ex situ XAS. The Co and Mn K-edges were examined using in situ XAS during charge or discharge from the initial P2-$Na_{2/3}Co_{2/3}Mn_{1/3}O_2$ phase. The Co and Mn L-edges and the O K-edge were examined by ex situ XAS. All of the sample spectra, with various sodium contents, are recorded in Figure 1.

Co and Mn K-Edges. The normalized XANES spectra at the Co and Mn K-edges for $Na_xCo_{2/3}Mn_{1/3}O_2$ are shown in Figure 2, together with those of $Co^{(II)}O$, $LiCo^{(III)}O_2$, $Mn^{(III)}{}_2O_3$,

dx.doi.org/10.1021/cm403597h | Chem. Mater. XXXX, XXX, XXX−XXX

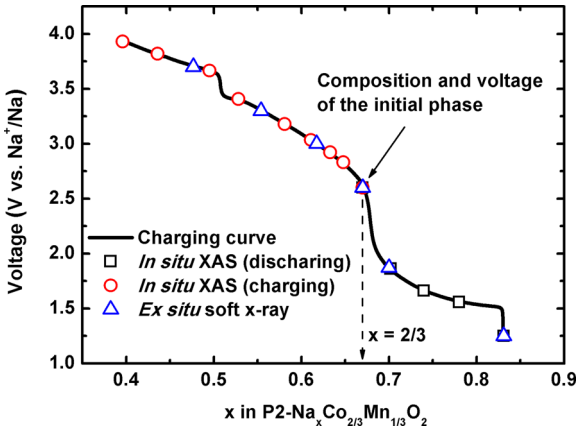

Figure 1. The charging curve of P2-$Na_{2/3}Co_{2/3}Mn_{1/3}O_2$; the points in "□", "○", and "△" represent the measuring points for the spectra of Co/Mn K-edge in the sodium intercalation process, in the sodium deintercalation process, and in ex situ soft X-ray (Co/Mn L-edge and O K-edge), respectively. The samples were preformed in different electrochemical process and then plotted in this charging curve according to their sodium contents and corresponding voltages.

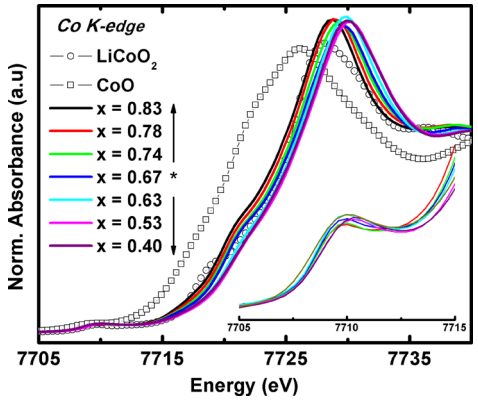

Figure 2. Normalized (a) Co and (b) Mn K-edge in situ XAS spectra of $Na_xCo_{2/3}Mn_{1/3}O_2$ obtained by transmission mode in comparison to those of reference materials. The insets are the zoom-in pre-edge region.

and $Li_2Mn^{(IV)}O_3$ as formal valences of reference compounds. The normalization both of charging and discharging processes shows consistent behavior (see Figure S3 (Supporting Information)).Weak pre-edge absorption peaks, corresponding to the transition of 1s core states to unoccupied 3d states, were observed at around 7710 eV for Co and 6542 eV for Mn (insets in Figure 2). The shoulders and main peaks of the absorption edge features are ascribed to the purely dipole-allowed 1s to 4p transition.[17] As shown in our previous study using magnetic susceptibility measurements, electron spin resonance (ESR), and ^{23}Na magic angle spinning nuclear magnetic resonance (MAS NMR) spectroscopy, only LS-Co^{3+} and Mn^{4+} ions are present in the initial $Na_{2/3}Co_{2/3}Mn_{1/3}O_2$ phase.[4] In agreement with these previous conclusions, the positions of the Co K- and Mn K-edges are close to those of Co^{3+} for $LiCoO_2$ and Mn^{4+} for Li_2MnO_3.

From the initial material $Na_{2/3}Co_{2/3}Mn_{1/3}O_2$, the x value was tuned by deintercalation/intercalation of sodium by an electrochemical process. As the amount of x decreased (x < 0.67), a shift of the Co K-edge could be observed toward higher energy. At the same time, the Mn K-edge remains at the same position as the starting phase. This indicates that the redox couple Co^{3+}/Co^{4+} contributes to the charge balance during the sodium deintercalation, similarly to the other cobalt system.[18] However, as the amount of intercalated sodium increases (x > 0.67), the Co and Mn K-edges both shift to lower energies, indicating that a reduction process occurs in both transition metal species during the discharge process. This behavior was unexpected, as we initially thought, in agreement with Wang et al.[16] that only the Mn^{4+}/Mn^{3+} redox couple would have been active.

Co and Mn $L_{II,III}$-Edges. To confirm this coreduction process, the Co and Mn $L_{II,III}$-edge X-ray absorption spectra were studied as they are relatively more sensitive to the oxidation state of transition metal ions, due to the electron dipole transition from the 2p core level to the 3d valence states.[19] The spectra obtained in total electronic yield (TEY) mode for $Na_xCo_{2/3}Mn_{1/3}O_2$ are shown in Figure 3. We focused

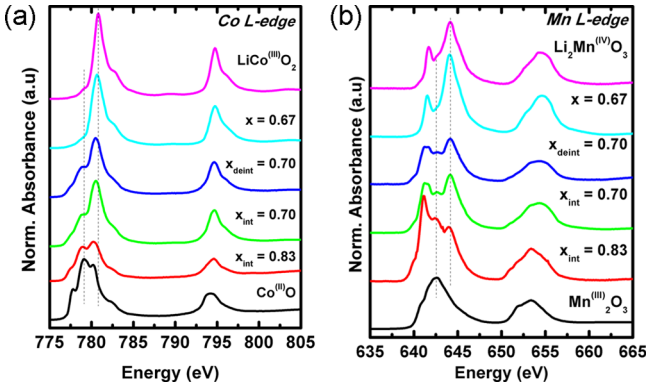

Figure 3. Normalized (a) Co and (b) Mn $L_{II,III}$-edge XAS spectra of $Na_xCo_{2/3}Mn_{1/3}O_2$ obtained by total electron yield (TEY) mode in comparison to those of reference materials.

here on the redox processes associated with the discharge of the batteries and therefore plotted only the spectra of the phase with $x \geq 2/3$. Spectra recorded for $x < 2/3$ are given in Figure S4 (Supporting Information), the evolution of which was in agreement with the oxidation of Co^{3+} in Co^{4+} during charging.

The spectra are dominated by Co 2p and Mn 2p core-hole spin orbit coupling, which splits each spectrum roughly into two parts: the transition from the $2p_{3/2}$ and $2p_{1/2}$ core levels to the unoccupied 3d level, the L_{III} (~777−785 eV for Co and ~640−648 eV for Mn) and the L_{II} (~ 793−798 eV for Co and~ 650−660 eV for Mn) white line regions. The line shape of the spectrum depends strongly on the multiplet structure given by the M 3d−3d and 2p−3d coulomb and exchange interactions, as well as by the local crystal fields and the hybridization with O 2p ligands.

Several $Na_xCo_{2/3}Mn_{1/3}O_2$ (x > 2/3) samples were studied: in the following designated here as "x_{int}", that is, the Na content of the phases obtained by Na intercalation from $Na_{2/3}Co_{2/3}Mn_{1/3}O_2$ (first discharge) and "x_{deint}" as the Na content of the phases obtained by Na deintercalation following the first discharge. Therefore, the reversibility of the intercalation/deintercalation process can be discussed by comparing x_{int} = 0.7 and x_{deint} = 0.7.

In the Co X-ray absorption spectra, two strong peaks at 794.6 and 780.6 eV (from the initial $Na_{2/3}Co_{2/3}Mn_{1/3}O_2$ phase) are due to absorption at the Co L_{II} and L_{III}-edges, that is, transitions from the $2p_{1/2}$ and $2p_{3/2}$ core levels to an

dx.doi.org/10.1021/cm403597h | Chem. Mater. XXXX, XXX, XXX−XXX

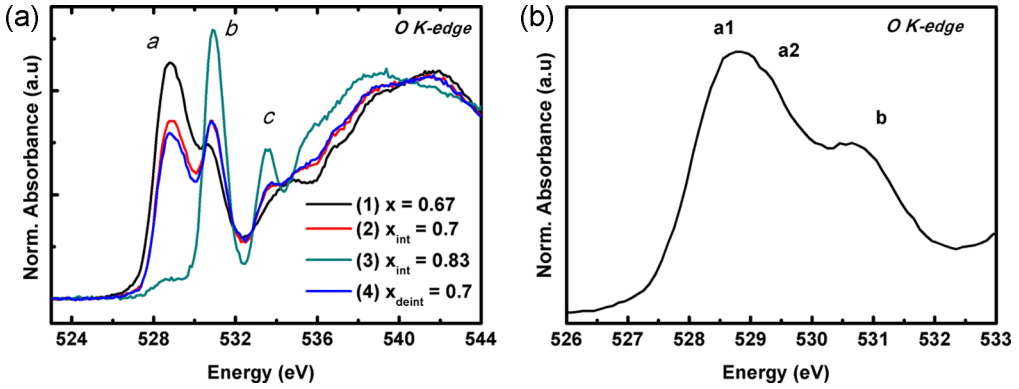

Figure 4. (a) The O K-edge XAS spectra in fluorescence yield (FY) mode for $Na_xCo_{2/3}Mn_{1/3}O_2$ during sodium intercalation process, and (b) zoom on the pre-edge of the O XAS spectrum of the $Na_{2/3}Co_{2/3}Mn_{1/3}O_2$ phase.

unoccupied 3d level. Both the position of the signals and their features look similar to those of the $LiCo^{(III)}O_2$ reference, implying that the cobalt ions are LS-Co^{3+}, this being in agreement with our previous studies. Upon Na-intercalation, two shoulders gradually appear at ca. 779.0 and 777.6 eV at the Co L_{III}-edge as seen for the x_{int} = 0.70 and x_{int} = 0.85 phases. These features look similar to those of $Co^{(II)}O$, indicating that some of the LS-Co^{3+} ions have been reduced to HS-Co^{2+} during discharge.

In the Mn X-ray absorption spectra, strong peaks located at 654.5 eV (L_{II}-edge) and two pronounced peaks, located at 644.0 and 641.6 eV (L_{III}-edge), are observed for the initial $Na_{2/3}Co_{2/3}Mn_{1/3}O_2$ phase and are assigned to Mn^{4+} ions by comparison to the $Li_2Mn^{(IV)}O_3$ reference (this is also in agreement with our previous studies). For the x_{int} = 0.70 and x_{int} = 0.85 samples on Na intercalation, a shoulder appears in the Mn L_{III}-edge spectra at around 642.6 eV. This shoulder can be assigned, by comparison with the $Mn^{(III)}{}_2O_3$ reference, to the formation of HS-Mn^{3+} ions.

These results provide evidence of the coexistence of Co^{3+}/Co^{2+} and Mn^{4+}/Mn^{3+} redox processes during Na intercalation in $Na_{2/3}Co_{2/3}Mn_{1/3}O_2$. This is in agreement with the shift to lower energy observed at the Co and Mn K-edges. Furthermore, the spectra recorded for the x_{deint} = 0.70 phase look similar to those for x_{int} = 0.70 at the Co and Mn L-edges, indicating a good reversibility of these two Co^{3+}/Co^{2+} and Mn^{4+}/Mn^{3+} redox processes.

For the behavior of $Na_xCo_{2/3}Mn_{1/3}O_2$, in which the sodium content x is lower than 2/3, it also shows a consistent trend with K-edge results in which only the Co^{3+}/Co^{4+} redox couple contributes to charge compensation during sodium deintercalation, as shown in Figure S4 (Supporting Information).

O K-Edge. The oxygen K-edge spectra of the $Na_xCo_{2/3}Mn_{1/3}O_2$ phases are shown in Figure 4. These spectra can be divided into different energy domains corresponding to various excitations from the O 1s core level. The first energy range (between 528 and 533 eV) corresponds to transitions that occur from O 1s to hybridized states between Co and Mn 3d and O 2p sub-bands leading the pre-edge peak (peaks labeled as "a" and "b" in Figure 4a). The peak energy (around 535 eV) can be assigned to transitions from the O 1s orbital to hybridized states between O 2p and Na 3p[20,21] (peak labeled as "c" in Figure 4a). Finally, the highest energy range (between 537 and 550 eV) corresponds to transitions toward hybridized levels between mixed Co 4sp and O 2p sub-bands.

The pre-edge peak includes one peak at 529.6 eV (labeled as "a") and a shoulder at 531.4 eV (labeled as "b") in the starting material x = 0.67. A closer look at the "a" peak indicates that it is actually split into two parts "a1" and "a2" (Figure 4b). In the literature, the peaks of the pre-edge have been assigned to transition toward empty t_{2g} or e_g orbitals.[20] In our case, a single peak would be expected for transitions to levels, implying O 2p orbitals mixed with Co 3d orbitals of LS-Co^{3+} ions in octahedral symmetry ($t_{2g}{}^6e_g{}^0$ configuration) as observed in $LiCoO_2$.[22] On the other hand, three peaks are expected for transitions to levels implying O 2p orbitals mixed with Mn 3d for a HS-Mn^{4+} ions in octahedral symmetry ($t_{2g}{}^3e_g{}^0$ configuration) as observed in MnO_2.[23] The O 1s XAS spectra of $Na_{2/3}Co_{2/3}Mn_{2/3}O_2$ can therefore be interpreted by considering LS-Co^{3+} and HS-Mn^{4+} ions in octahedral sites. One can tentatively interpret such a near-edge structure by neglecting the influence of the O 1s core hole.[24] To attribute peaks, we need to get an idea of the relative positions of the empty Co and Mn levels. We thus computed the Spin Density of States (DOS) of this compound by DFT calculation using the GGA method. A model P2-$Na_{2/3}Co_{2/3}Mn_{1/3}O_2$ compound was considered, and its structure is given in Figure S1 (Supporting Information). Figure 5 gives the resulting spin DOS: Total DOS (Figure 5a), partial DOS on the Co and Mn 3d levels (Figure 5b), and partial DOS on the O 2p levels (Figure 5c) are plotted. The schematic view of the relative position in energy of the filled and empty e_g and t_{2g} levels in P2-$Na_{2/3}Co_{2/3}Mn_{1/3}O_2$ based on the Density of States calculations is shown in Supporting Information Figure S5. As seen in Figure 5b, the position of the Fermi level is in agreement with the stabilization of LS-Co^{3+} and HS-Mn^{4+} ions in the compound. Among the empty levels, just above the Fermi levels, resulting from the hybridization of the M 3d and O 2p orbitals, we observed that the empty Co and Mn $e_g(\uparrow)$ orbitals and the empty Co $e_g(\downarrow)$ and the empty Mn $t_{2g}(\downarrow)$ orbitals are located roughly at the same energy (Figure 5b). The Mn $e_g(\downarrow)$ levels are located at higher energy and clearly separated from the other levels by almost 1 eV. As the O K-edge spectra reflect transitions toward empty O 2p orbitals mixed with M 3d ones, we also plotted the partial O 2p DOS and observe then the O 2p contributions to the different t_{2g} and e_g levels mentioned above (Figure 5c). On the basis of this analysis, one can therefore suggest the assignment of the pre-edge O1s XAS peaks of $Na_{2/3}Co_{2/3}Mn_{2/3}O_2$ represented in Figure 4b as follows: the peak at 531.4 eV, labeled as "b", can be assigned to transitions to O 2p mixed with Mn $e_g(\downarrow)$ orbitals, which is

dx.doi.org/10.1021/cm403597h | Chem. Mater. XXXX, XXX, XXX−XXX

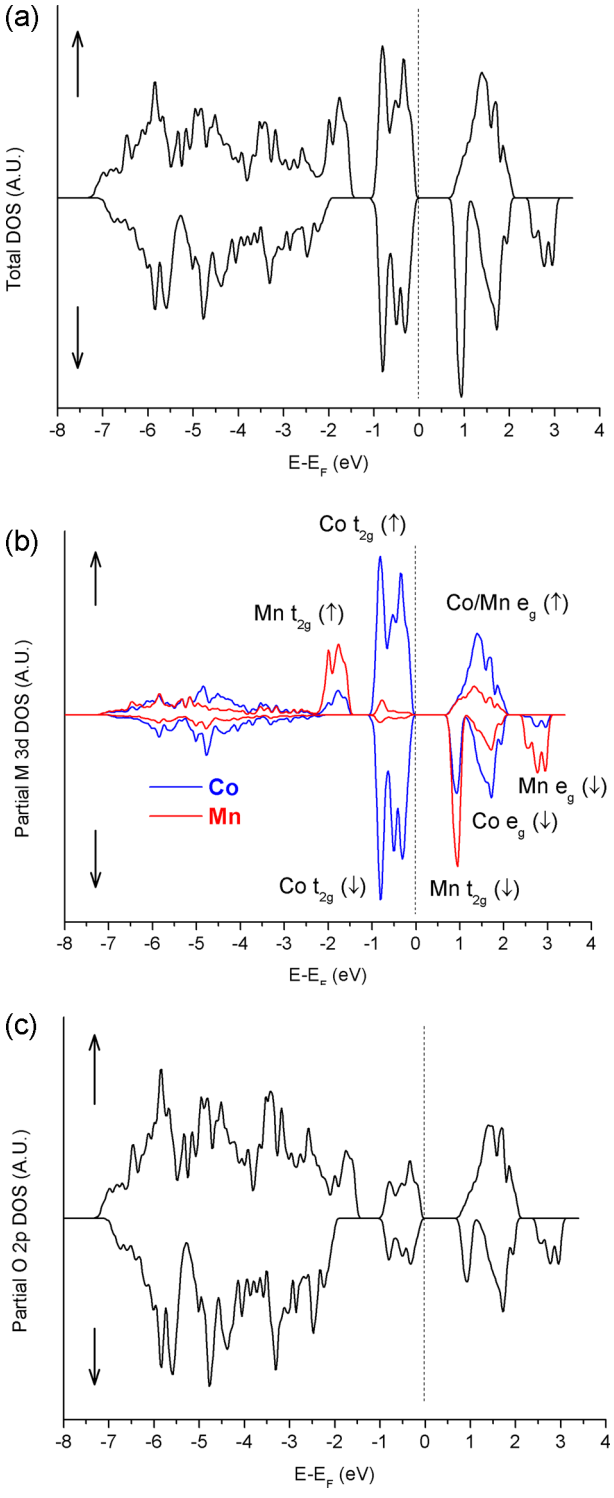

Figure 5. Calculated spin DOS of $Na_{2/3}Co_{2/3}Mn_{1/3}O_2$: (a) total, (b) partial on Co and Mn 3d orbitals, and (c) partial on O 2p orbitals.

clearly located at higher energy, and the peaks around 529.6 eV, labeled as "a", can be assigned to transitions to O 2p mixed with Co and Mn $e_g(\uparrow)$ orbitals, Co $e_g(\downarrow)$ and Mn $t_{2g}(\downarrow)$ orbitals. The "a1" and "a2" fine structure observed could be due either to the different contributions observed in the DOS in this region and/or to a splitting of the Mn $t_{2g}(\downarrow)$ orbitals clearly observed in Figure 5b. This splitting is due to a lifting of degeneracy of the t_{2g} because of a flattening of the MnO_6 octahedra along the c axis leading to a D_{3d} local symmetry instead of O_h: the three t_{2g} split into 2 e_g' levels and one a_{1g}.[20]

Upon sodium intercalation, in the pre-edge region, the intensity of peak "a" decreases and that of peak "b" increases as observed for the t = 0.70 and x_{int} = 0.85 phases. According to our assignment, this would suggest that the number of empty levels involving O 2p mixed with Co and Mn $e_g(\uparrow)$ orbitals, Co $e_g(\downarrow)$ and Mn t_{2g} $(\downarrow)$ orbitals decreases; this assignment suggests the formation of HS-Co^{2+} $(t_{2g}^5e_g^2)$ and HS-Mn^{3+} $(t_{2g}^3e_g^1)$ ions that exhibit less unoccupied e_g states. The strong modification of the O K edge spectra upon Na intercalation clearly indicates a strong modification of the hybridization between O 2p and M 3d. Upon Na intercalation, the peak labeled as "c" in Figure 4a increases in intensity gradually from x_{int} = 0.67 to x_{int} = 0.85, as the amount of Na increases as expected from the assignment of this peak to hybridized states between O 2p and Na 3p. The spectrum recorded for the x_{deint} = 0.70 phase looks similar to that of x_{int} = 0.70 at the O K-edge; this is similar to the conclusions with respect to the Co and Mn L-edges, in addition to which a good reversibility of the redox processes is observed.

The O K-edge spectra of the $Na_xCo_{2/3}Mn_{1/3}O_2$ with $x \leq 2/3$ are shown in Figure S5 (Supporting Information). As x decreases from x = 2/3, the global shape of the spectra is maintained, but the pre-edge shifts slightly to lower energy position. This is in agreement with the increase of covalency expected for the Co−O bond as Co^{3+} is oxidized to Co^{4+}. As the covalency increases, as x decreases, we observe an increase of the participation of O in the redox process during charging.

EXAFS. The local environments of Co and Mn were studied by EXAFS. The k^3-weighted Fourier transform (FT) magnitude spectra of the Co and Mn K-edges for $Na_xCo_{2/3}Mn_{1/3}O_2$ as a function of sodium content (x) are shown in Figure 6. The peak located at ca. 1.9 Å is assigned to the first coordination shell, which represents the metal to oxygen M−O bonding. The second peak at ca. 2.8 Å is the contribution of a six-coordinated transition metal Co/Mn atom on the transition metal layer.

Detailed results such as bond length and the Debye−Waller factor, extracted by fitting, are given in Figure 7 and Figure S7 (Supporting Information). The goodness of fit for selected data points is shown in Figure S8 (Supporting Information), and the structural parameters are listed in Table S8 (Supporting Information). The Na intercalated ($x \geq 2/3$) bond lengths of Co−O and Mn−O show complex behavior. The bond length of Mn−O and Co−O first decreases slightly as the sodium content (x) increases to x = 0.74 and then increases again as the sodium content (x) increases to 0.83. This complex scheme could be due to a strong local distortion of the adjacent MO_6 octahedron, as the Mn^{3+} ions are Jahn−Teller active.[25] In our case, only one path for the M−O bond in the first shell, which originated from the structure of initial phase P2−$Na_{2/3}Co_{2/3}Mn_{1/3}O_2$, was considered to fit the EXAFS results; however, a distorted MO_6 octahedron may result in two different M−O distances. Therefore, the competition of the two M−O lengths could contribute to this complex scheme.[26] For the Co−M and Mn−M bonds, the trends are clearer; that is, both of them increase upon Na intercalation, which is in agreement with our previous study that shows an increase in the a-cell parameter derived from XRD refinements.[4] The Debye−Waller factors for Co−O, Mn−O, Co−M, and Mn−M all increase during sodium intercalation. This also indicates that the structure of the $Na_xCo_{2/3}Mn_{1/3}O_2$ becomes more distorted.

dx.doi.org/10.1021/cm403597h | Chem. Mater. XXXX, XXX, XXX−XXX

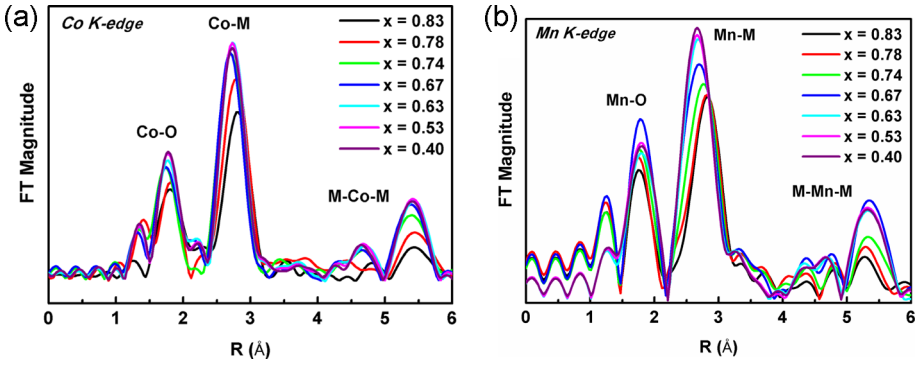

Figure 6. The k^3-weighted Fourier transform magnitudes of the (a) Co and (b) Mn K-edge EXAFS spectra during the sodium intercalation process.

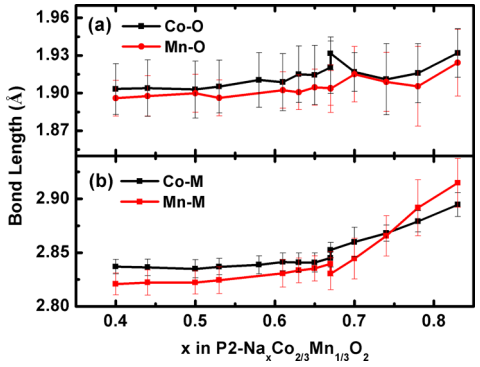

Figure 7. The EXAFS fitting results for Co and Mn K-edge: (a) metal−O bond length and (b) metal to metal bond length.

CONCLUSION

The charge compensation mechanism for $Na_xCo_{2/3}Mn_{1/3}O_2$ was investigated by both ex situ and in situ X-ray absorption spectroscopy during the discharging process. The electronic transitions at the O K-edge were successfully assigned by combining DFT computation and X-ray absorption spectroscopy. The oxidation states in pristine $Na_{2/3}Co_{2/3}Mn_{1/3}O_2$ of Co and Mn are assigned as +3 and +4, respectively. Important features of Co^{2+} and Mn^{3+}, for example, energy shift and bond distance, observed using XAS upon sodium intercalation, indicate that the redox pairs of both Co^{3+}/Co^{2+} and Mn^{4+}/Mn^{3+} are simultaneously involved in the charge compensation process. This result is very helpful, enabling us to understand the mechanisms occurring during the discharge of overlithiated $Li_{1+x}(Ni,Mn,Co)O_2$ phases, suggesting that at the end of the discharge at low voltage some of the cobalt could be reduced to the divalent state simultaneously with the Mn^{4+} to Mn^{3+} reduction. This point, regarding the fact that two metals can be simultaneously active, in contrast to the widely reported view that only one metal is active, has not been widely considered in the literature and is we believe worthy of future investigation.

ASSOCIATED CONTENT

Supporting Information

Details of structure parameters, computation model, normalization of XAS spectra, and curve-fitting for EXAFS (PDF). This material is available free of charge via the Internet at http://pubs.acs.org.

AUTHOR INFORMATION

Corresponding Authors

*E-mail: carlier@icmcb-bordeaux.cnrs.fr.
*E-mail: bjh@mail.ntust.edu.tw.

Notes

The authors declare no competing financial interest.

ACKNOWLEDGMENTS

This work benefited from grants awarded by the Agence Nationale de la Recherche (Blanc Inter II, SIMI 8) no. 2011-IS08-001-01, the Ministry of Economic Affairs of Taiwan (101-EC-17-A-08-S1-183), and the Joint project between French National Research Agency and the National Science Council of Taiwan (ANR-NSC-101-2923-E-011-001-MY3, LaNaMOx), while Région Aquitaine and CNRS are also acknowledged for B.M. scholarship. C. Denage, and P. Dagault are acknowledged for experimental support. We thank L. Croguennec, O. Toulemonde, and R. Berthelot for fruitful discussions. The Mésocentre de Calcul Intensif Aquitain (MCIA) is acknowledged for providing computing facilities, and P. Aurel (ISM) is acknowledged for technical assistance. Special thanks to Dr. John D. Rick for help with proofreading.

REFERENCES

(1) Prado, G.; Fournès, L.; Delmas, C. *J. Solid State Chem.* **2001**, *159*, 103−112.
(2) Guerlou-Demourgues, L.; Fournès, L.; Delmas, C. *J. Electrochem. Soc.* **1996**, *143*, 3083−3088.
(3) Croguennec, L.; Dedryvere, R.; Menetrier, M.; Komaba, S.; Morcrette, M.; Carlier-Larregaray, D.; Willmann, P.; Gonbeau, D.; Delmas, C. Redox Processes in $T^{\#}2/O_6$-$Li_xCo_{2/3}Mn_{1/3}O_2$ Part 1: XANES and XPS Studies. *International Meeting on Lithium-ion Batteries (IMLB-2006)*; Biarritz, 2006.
(4) Carlier, D.; Cheng, J. H.; Berthelot, R.; Guignard, M.; Yoncheva, M.; Stoyanova, R.; Hwang, B. J.; Delmas, C. *Dalton Trans.* **2011**, *40*, 9306−12.
(5) Tsai, Y. W.; Lee, J. F.; Liu, D. G.; Hwang, B. J. *J. Mater. Chem.* **2004**, *14*, 958.
(6) Tsai, Y. W.; Hwang, B. J.; Ceder, G.; Sheu, H. S.; Liu, D. G.; Lee, J. F. *Chem. Mater.* **2005**, *17*, 3191−3199.
(7) Yabuuchi, N.; Kajiyama, M.; Iwatate, J.; Nishikawa, H.; Hitomi, S.; Okuyama, R.; Usui, R.; Yamada, Y.; Komaba, S. *Nat. Mater.* **2012**, *11*, 512−7.
(8) Roisnel, T.; Rodríquez-Carvajal, J. *Mater. Sci. Forum* **2001**, *378*−*381*, 118−123.
(9) Sayers, D. E. *Report of the International XAFS Society Standards and Criteria Committee*, 2000.
(10) Ravel, B.; Newville, M. *J. Synchrotron Radiat.* **2005**, *12*, 537−41.
(11) McBreen, J. *J. Solid State Electrochem.* **2008**, *13*, 1051−1061.

(12) de Groot, F. M. F.; Arrio, M. A.; Sainctavit, P.; Cartier, C.; Chen, C. T. *Physica B: Condens. Matter* **1995**, *208*−*209*, 84−86.
(13) Kresse, G.; Furthmüller, J. *Comput. Mater. Sci.* **1996**, *6*, 15−50.
(14) Kresse, G.; Joubert, D. *Phys. Rev. B* **1999**, *59*, 1758.
(15) Blöchl, P. E. *Phys. Rev. B* **1994**, *50*, 17953−17979.
(16) Wang, X.; Tamaru, M.; Okubo, M.; Yamada, A. *J. Phys. Chem. C* **2013**, *117*, 15545−15551.
(17) Juhin, A.; de Groot, F.; Vankó, G.; Calandra, M.; Brouder, C. *Phys. Rev. B* **2010**, *81*, 11.
(18) Ding, J. J.; Zhou, Y. N.; Sun, Q.; Yu, X. Q.; Yang, X. Q.; Fu, Z. W. *Electrochim. Acta* **2013**, *87*, 388−393.
(19) Yang, W.; Liu, X.; Qiao, R.; Olalde-Velasco, P.; Spear, J. D.; Roseguo, L.; Pepper, J. X.; Chuang, Y.-d.; Denlinger, J. D.; Hussain, Z. *J. Electron Spectrosc. Relat. Phenom.* **2013**.
(20) Wu, W. B.; Huang, D. J.; Okamoto, J.; Tanaka, A.; Lin, H. J.; Chou, F. C.; Fujimori, A.; Chen, C. T. *Phys. Rev. Lett.* **2005**, *94*, 146402.
(21) Kroll, T.; Knupfer, M.; Geck, J.; Hess, C.; Schwieger, T.; Krabbes, G.; Sekar, C.; Batchelor, D. R.; Berger, H.; Büchner, B. *Phys. Rev. B* **2006**, *74*, 115123.
(22) van Elp, J.; Wieland, J. L.; Eskes, H.; Kuiper, P.; Sawatzky, G. A.; de Groot, F. M. F.; Turner, T. S. *Phys. Rev. B* **1991**, *44*, 6090−6103.
(23) Kurata, H.; Colliex, C. *Phys. Rev. B* **1993**, *48*, 2102−2108.
(24) van Elp, J.; Tanaka, A. *Phys. Rev. B* **1999**, *60*, 5331−5339.
(25) Thackeray, M. M.; David, W. I. F.; Bruce, P. G.; Goodenough, J. B. *Mater. Res. Bull.* **1983**, *18*, 461−472.
(26) Hwang, B. J.; Tsai, Y. W.; Santhanam, R.; Liu, D. G.; Lee, J. F. *J. Electrochem. Soc.* **2003**, *150*, A335.